Sensors & Diagnostics

PAPER

View Article Online
View Journal | View Issue

Cite this: *Sens. Diagn.*, 2025, **4**, 1114

MRI-based radiomic signature for MYCN amplification prediction of pediatric abdominal neuroblastoma

Xuan Jia,†[a] Junjie Wen, †[ba] Jiawei Liang,[a] Xiaohui Ma,[a] Wenqi Wang,[a] Jinhu Wang*[cde] and Yi Zhang*[ba]

Received 5th June 2025,
Accepted 5th September 2025

DOI: 10.1039/d5sd00089k

rsc.li/sensors

MYCN gene amplification critically drives neuroblastoma aggressiveness and poor outcomes, necessitating precise preoperative identification to guide risk-adapted therapies. Current invasive detection methods present substantial challenges for pediatric patients. To address this unmet need, we developed a noninvasive MRI-based radiomic signature for predicting MYCN amplification status in childhood abdominal neuroblastoma. In this prospective study, 99 patients with pathologically confirmed abdominal neuroblastoma underwent preoperative MRI between April 2019 and September 2021. From T2-weighted images, 1409 radiomic features were extracted per subject. Through two-sample statistical testing and least absolute shrinkage and selection operator (LASSO) regression, we constructed an optimized radiomic signature incorporating six highly discriminative features. The signature achieved exceptional performance (AUC = 0.91) in predicting MYCN amplification, significantly outperforming neuron-specific enolase levels (AUC = 0.68, p-value < 0.001) and all individual radiomic features. When integrated with neuron-specific enolase *via* multivariate logistic regression, the model achieved comparable performance (AUC = 0.91) to the signature only. Our findings establish the clinical viability of this MRI-based approach for noninvasively stratifying MYCN amplification status, offering significant potential to optimize surgical planning and therapeutic strategies for pediatric neuroblastoma.

Introduction

Neuroblastoma (NB) is a malignant embryonal tumor originating from the postganglionic sympathetic ganglia.[1] It is common in children aged 1 to 5 years, easy to metastasize, and has a poor prognosis.[2] Several studies have revealed the molecular characteristics of NB that about 25% of NB children have MYCN gene amplification, which drives the occurrence of high-frequency mutations in tumors and is closely related to high-risk grouping and poor prognosis.[3,4] Therefore, it is necessary to assess the MYCN status in diagnosing NB patients for tailored treatments to improve their clinical outcomes. However, the MYCN status is usually obtained by pathological biopsy of tumor samples, which is invasive and may cause complications or bleeding in pediatric patients.[5] In addition, the MYCN gene status cannot be determined in most NB tumors at the initial diagnosis, which seriously affects risk stratification results and treatment strategies. Children exhibiting upregulation of this oncogene are automatically placed in the high-risk group before treatment begins, independent of other disease characteristics, and generally need targeted therapeutic interventions.[6] Hence, it is of great clinical significance to explore a non-invasive method suitable for children to predict MYCN expansion.

Radiomics is an emerging technology that employs data characterization algorithms to automate the quantitative analysis of a series of radio-phenotypic characteristics that potentially reflect biological properties of the pathology, clinical phenotypes, and genetic and molecular markers.[7,8] Recent studies have confirmed the potential of radiogenomics analysis based on computed tomography (CT) to predict various tumor-specific genes,[9,10] but this examination method is injurious for children.[11] Magnetic resonance imaging (MRI) is a radiation-free examination

[a] *Department of Radiology, Children's Hospital, Zhejiang University School of Medicine, Hangzhou, Zhejiang, China*
[b] *Key Laboratory for Biomedical Engineering of Ministry of Education, Department of Biomedical Engineering, College of Biomedical Engineering & Instrument Science, Yuquan Campus, Zhejiang University, Room 418, Teaching Building 6, 38 Zheda Road, Hangzhou, Zhejiang, 310027, China. E-mail: yizhangzju@zju.edu.cn; Tel: +86 15857193376*
[c] *Department of Surgical Oncology, Children's Hospital Zhejiang University School of Medicine, 3333 Binsheng Road, Hangzhou 310051, China. E-mail: wjh@zju.edu.cn; Tel: +86 13067748567*
[d] *Pediatric Cancer Research Center, National Clinical Research Center for Child Health, Hangzhou, China*
[e] *Cancer Center, Zhejiang University, Hangzhou, China*
† Xuan Jia and Junjie Wen contributed equally to this work.

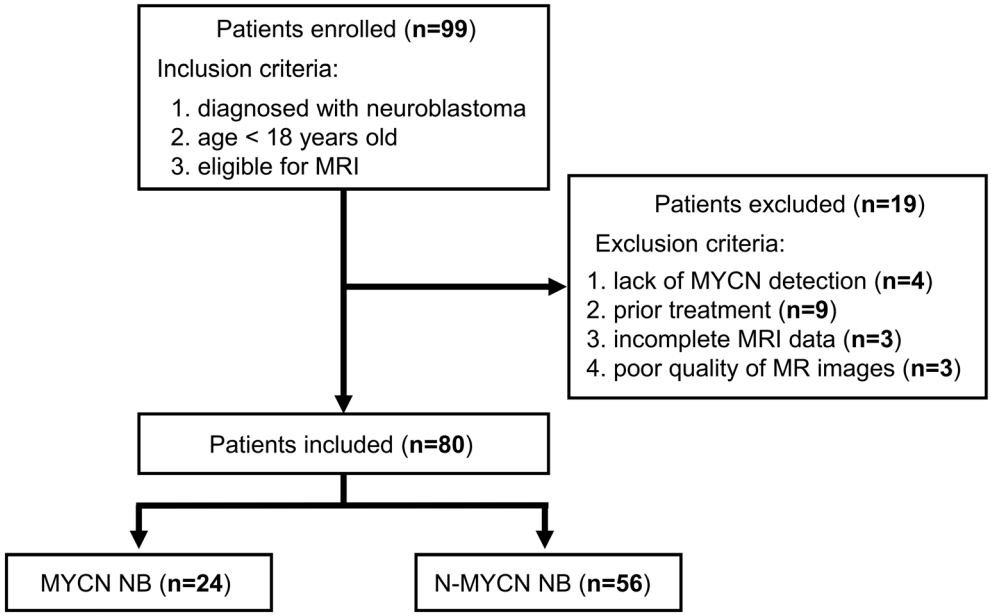

Fig. 1 Flow chart of patient selection.

method, which has been used to diagnose and characterize neuroblastoma in previous studies.[12–14] In addition, the MRI-based radiomic analysis method has played an important role in characterizing various types of tumors[15–17] and has improved patients' diagnoses.

The study aims to establish a radiomic signature based on MRI, evaluate its feasibility of predicting MYCN amplification in children with abdominal NB, and compare its performance with the neuron-specific enolase (NSE) level often used in clinical practice.

Materials and methods

Subjects

Our research has been performed in accordance with the Declaration of Helsinki, and was reviewed and approved by the Ethics Committee of the Children's Hospital Affiliated to Zhejiang University School of Medicine, and all guardians of the subjects understood the contents of the examination before conduction and signed the informed consent form (2021-IRB-117).

A cohort of 99 patients diagnosed with abdominal NB were consecutively enrolled in this study from April 2019 to September 2021 and underwent abdominal MRI examinations. The flow chart of the patient selection process is shown in Fig. 1. The inclusion criteria were: (1) diagnosed with pathologically confirmed NB; (2) ≤18 years old at diagnosis; and (3) eligible for MRI. The exclusion criteria were: (1) lack of MYCN detection; (2) incomplete MRI data; (3) prior treatment before MRI examination; and (4) poor quality of MR images.

MYCN assessment

The MYCN status was evaluated by fluorescence *in situ* hybridization (FISH) using a two-color probe and with a CEP2 centromeric probe as a reference, and MYCN amplification was only considered when it increased 4-fold compared to the reference value.[18] According to the presence/absence of MCYN amplification, the included patients with abdominal NB were divided into two subgroups: with and without MYCN amplification.

Imaging protocols

All subjects underwent MRI examinations on a 3T scanner (Achieva, Philips Healthcare). Patients under 5 years were sedated. A 10% chloral hydrate solution was administered

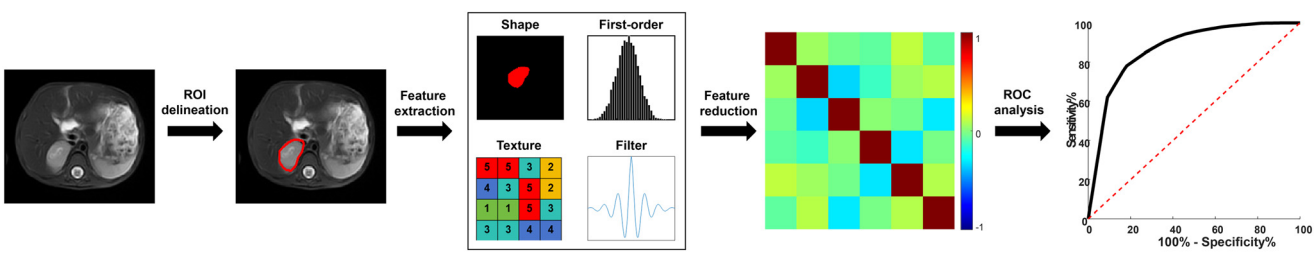

Fig. 2 Flowchart of the whole processing pipeline.

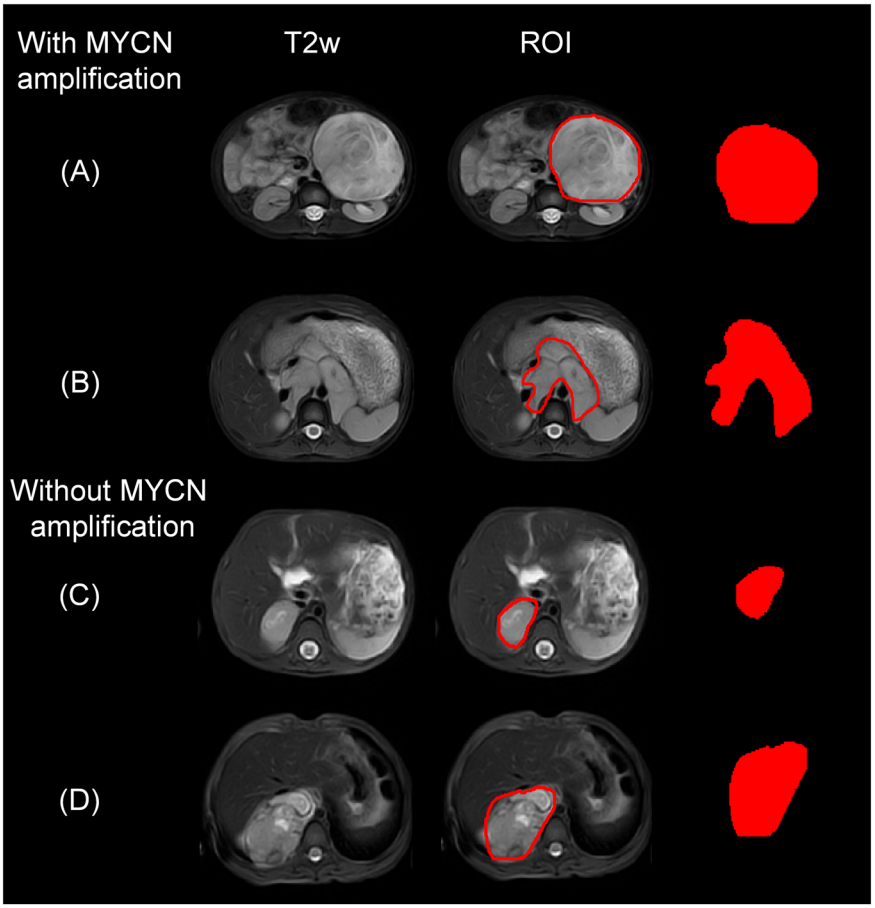

Fig. 3 Anatomical T2w images and manual segmentation of T2w regions of interest (ROI) from four neuroblastoma patients. Rows (A) and (B) display a 5-year-old girl and a 6-year-old girl with MYCN amplification, respectively. Rows (C) and (D) show a 6-year-old girl and a 4-year-old boy without MYCN amplification, respectively.

either *via* an enema or orally about 40 min before the examination, with the scan being conducted while the patient was asleep. Considering the issue of patient cooperation, the data collection time needs to be as short as possible, and thus only the pre-contrast T1-weighted (T1w) and T2-weighted (T2w) sequences were executed. The total time for completing the MR examination was ~15 minutes. All MR images were retrieved from the picture archiving and communication system (PACS) for subsequent processing and analysis. Given that T2w images provide better visualization of neuroblastoma lesions, subsequent processing and analysis were conducted exclusively on T2w images.

Habitat definition and processing

The workflow of this study is shown in Fig. 2. The MRI data were loaded from the PACS system and the region of interest (ROI) was delineated manually on the transverse T2w images using the semi-automatic segmentation method in the 3D Slicer software[19] by two pediatric radiologists both with more than 15 years of clinical experience. Each observer delineated the ROI three times and measured the average. The average results of the two observers were used as the final data. Intra- and inter-observer consistency coefficients (ICCs) were used to evaluate the differences of features extracted from different ROIs. An ICC greater than 0.8 was considered to have good consistency. The T2w images and ROIs of four NB patients with and without MYCN amplification are displayed in Fig. 3.

Table 1 Comparison of clinical features in patients with neuroblastoma

Subgroup	MYCN	N-MYCN	*P* value
No. of patients	24	56	—
Age in months at diagnosis			
Mean	50.7	44.9	0.47
Median	43.5	35.0	
Range	[3165]	[2132]	
SD	35.5	31.6	
Male	11	29	0.62
Female	13	27	
NSE (ng ml^{-1})			
Mean	80.58	35.48	0.003*
SD	99.60	33.36	

Abbreviations: SD, standard deviation; MYCN, with MYCN amplification; N-MYCN, without MYCN amplification. * stands for the p-value < 0.05.

Table 2 The six radiomic features retained after feature selection

Filter	Category	Feature	Frequency
Wavelet-LLH	GLRLM	RunLengthNonUniformityNormalized	0.856
Wavelet-HHL	First order	Skewness	0.820
Wavelet-HLL	GLCM	ClusterShade	0.732
Gradient	GLCM	Correlation	0.338
Wavelet-LLL	NGTDM	Busyness	0.296
Wavelet-HHH	GLRLM	HighGrayLevelRunEmphasis	0.284

Radiomic feature extraction

The open-source Python package (PyRadiomics)[20] was used to extract radiomic features within the tumor ROI on images from abdominal NB in children. The original MR images first underwent N4 bias field correction, and then were subjected to isotropic voxel resampling and signal intensity normalization.[21] Then, the preprocessed images were applied with multiple filters including Wavelet, Laplacian of Gaussian (LoG), Square, SquareRoot, Logarithm, and Exponential, *etc.* for transformation. Images before and after filtering both went through the feature extraction workflow. A total of 1409 radiomic features were extracted from each patient's original MR images and filter-transformed ones. All extracted features were standardized using *z*-score normalization for further analysis.

Statistical analysis

All statistical analyses were performed with MATLAB (R2021b, MathWorks). The differences between subgroups in age and gender were assessed with a two-sample independent *t*-test and chi-square test, respectively. The NSE level difference between subgroups was also evaluated using a two-sample independent *t*-test. We performed 100 iterations of 5-fold cross-validation split to ensure robust results and mitigate the impact of random partitioning. The following feature selection was performed on the training set only. The Shapiro–Wilk test was used to evaluate the normality of all extracted radiomic features. The two-sample independent *t*-test (for data following a normal distribution) and rank sum test (for data not following a normal distribution) were performed to select the features that exhibited significant differences in the MYCN amplification status between groups. The features with a *p*-value below 0.05 were retained for further selection. The least absolute shrinkage and selection operator (LASSO) algorithm was used for further feature screening.[22] Due to the number of the training set, up to six radiomic features were retained as a feature subset in each fold of each iteration.[23] Then, we tallied the frequency of each feature across all subsets and selected the top six as the final feature set. The Pearson correlation coefficient was used to assess the collinearity and redundancy between the retained radiomic features. We performed another 100 iterations of 5-fold cross-validation split for model construction. In each fold of each iteration, a LASSO model was trained using the training set, and the radiomic signature was derived as a linear combination of the six features from the testing set and their corresponding coefficients determined by the LASSO model. The performance of each retained radiomic feature, NSE level, and radiomic signature was assessed by the receiver operating characteristic curve (ROC) analysis. In addition, the radiomic signature was combined with the NSE level using a multivariate logistic regression model for exploring whether the NSE level could provide additional value. The performance was assessed based on the average area under

Table 3 Comparison of the six retained radiomic features after feature selection between two subgroups

Feature	MYCN	N-MYCN	*P* value
F1	0.096 ± 0.024	0.081 ([0.046, 0.110])	0.003*
F2	0.075 ± 0.187	−0.089 ± 0.176	<0.001*
F3	−696.8 ± 1375.1	312.5 ± 1275.7	0.002*
F4	0.627 ([0.531, 0.735])	0.670 ([0.563, 0.815])	0.009*
F5	0.003 ± 0.003	0.002 ± 0.001	0.004*
F6	2.503 ([2.484, 2.528])	2.497± 0.011	0.01*

Abbreviations: MYCN, with MYCN amplification; N-MYCN, without MYCN amplification; F1–6 represent the six features in Table 2. * stands for the *p*-value < 0.05. Footnote: data that follow a normal distribution are presented as mean ± standard deviation, and those that do not follow a normal distribution are presented as median (range).

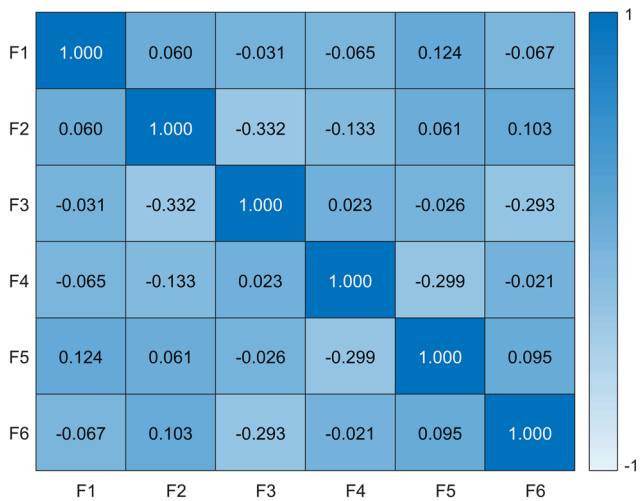

Fig. 4 The heatmap of the correlation coefficient between the 6 radiomic features retained. F1–6 represent the six features in Table 2.

Table 4 The performance of the single retained radiomic features for predicting MYCN amplification of abdominal NB across 100 runs of 5-fold cross-validation

Feature	PPV	NPV	Sensitivity	Specificity	AUC
F1	0.76	0.80	0.42	0.94	0.72
F2	0.76	0.83	0.53	0.92	0.76
F3	0.56	0.83	0.57	0.82	0.75
F4	0.54	0.80	0.47	0.85	0.70
F5	0.67	0.78	0.34	0.93	0.67
F6	0.75	0.79	0.39	0.94	0.69

Abbreviations: F1–6 represent the six features in Table 2.

the ROC curve (AUC), positive predicted value (PPV), negative predicted value (NPV), sensitivity, and specificity computed over 100 repeated testing sets. The statistical significance of the differences between the AUC values was assessed with the Delong test method.[24] The p-value below 0.05 indicates statistical significance in all tests.

Results and discussion

Patient demographics

As presented in Fig. 1, among the 99 neuroblastoma patients enrolled, 4 subjects were excluded due to lack of MYCN results, 9 subjects excluded owing to prior treatment about NB, 3 subjects excluded because of incomplete MRI data, and 3 subjects excluded for poor image quality. For the 80 patients finally included in this study, 24 cases had MYCN amplification and 56 cases did not have MYCN amplification. There were no significant differences between the two subgroups in age and gender. In contrast, the NSE level exhibited a significant difference between the two subgroups. Patients' demographics are listed in Table 1.

Feature selection

The intra- and inter-observer consistency coefficients of the features extracted from different ROIs were 0.91 and 0.84, respectively. Among the 1409 radiomic features extracted, 6 features were retained after feature selection, including 1 first order feature, 2 GLCM features, 2 GIRLM features, and 1 NGTDM feature (Table 2). As displayed in Table 3, these features were significantly different between patients with and without MYCN amplification (p values < 0.05), with their frequencies across all feature subsets shown in Table 2. Fig. 4 shows the heatmap of the correlation coefficient between the 6 radiomic features retained.

Comparison and predicting performance of single radiomic features

Table 3 shows the differences in the 6 radiomic features retained between the two subgroups. Radiomic features that follow a normal distribution are presented as mean ± standard

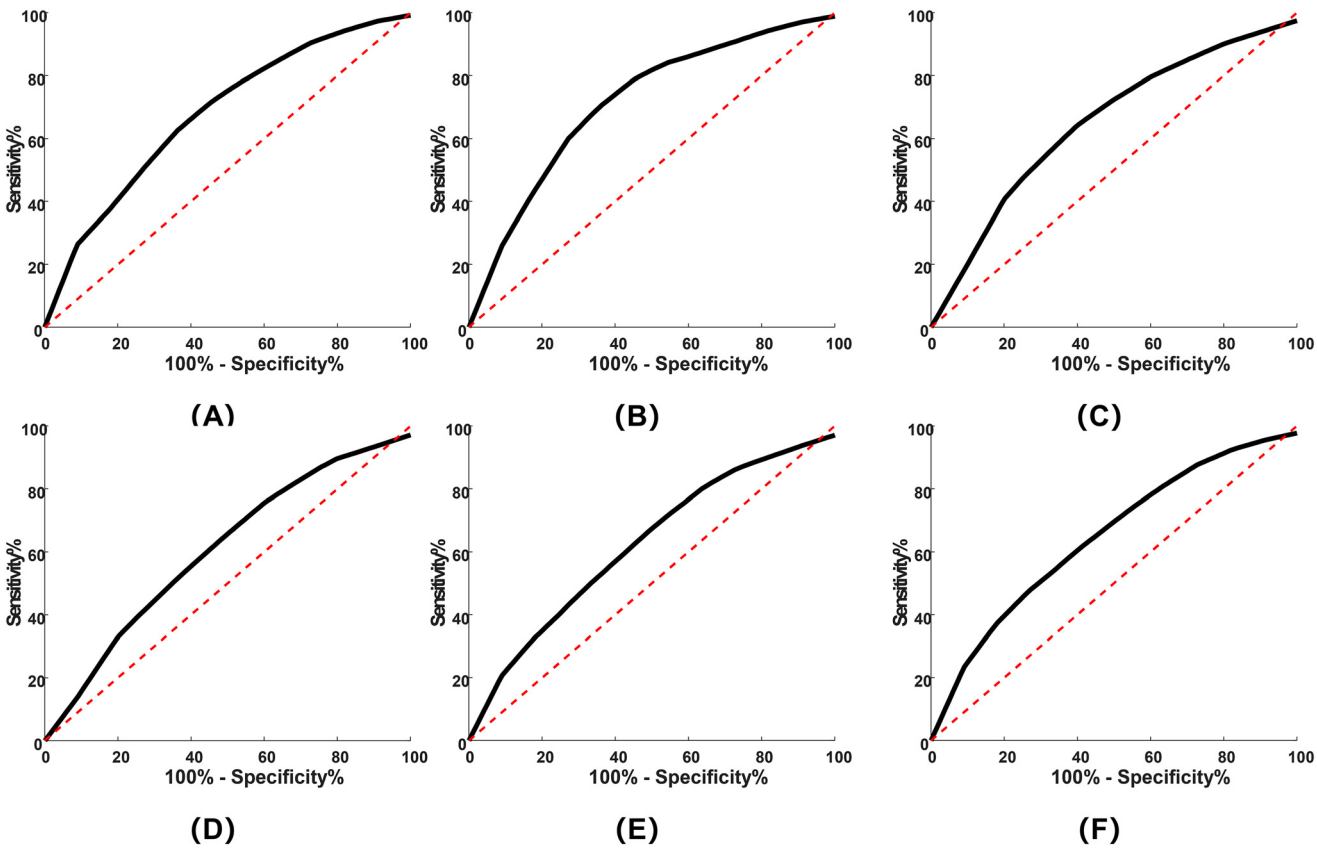

Fig. 5 ROC curves of single radiomic features retained for predicting MYCN amplification of abdominal NB. (A)–(F) correspond to F1–6 in Table 4.

Table 5 The performance of the NSE level, radiomic signature, and combined model for predicting MYCN amplification of abdominal NB across 100 runs of 5-fold cross-validation

Factor	PPV	NPV	Sensitivity	Specificity	AUC
NSE	0.79	0.79	0.40	0.95	0.68
Rad	0.95	0.90	0.73	0.97	0.91
Rad + NSE	0.94	0.91	0.76	0.97	0.91

Abbreviations: Rad, radiomic signature.

deviation, and those that do not follow a normal distribution are presented as median (range). Table 4 presents the performance of each radiomic feature for predicting MYCN amplification in pediatric NB patients over 100 repeated testing sets. The corresponding ROC curves of those features are shown in Fig. 5. The skewness of the wavelet-HHL transformed image was the best one with an AUC of 0.76 (p values < 0.01 compared with other features, except the ClusterShade of the wavelet-HLL transformed image) for predicting MYCN amplification.

Comparison of the predicting performance between the radiomic signature and NSE level

As displayed in Table 5, the NSE level achieved an AUC of 0.68 for predicting MYCN amplification in abdominal NB across 100 repeated testing sets. In comparison, the radiomic signature obtained by a linear combination of the 6 radiomic features yielded a significantly higher AUC of 0.91 (p-value $<$ 0.001). Furthermore, the radiomic signature performed significantly better than the single radiomic features (p values $<$ 0.001). In addition, the multivariate logistic regression model combined the NSE level and radiomic signature and achieved comparable performance (AUC = 0.91) to the signature only (p-value = 0.07) for predicting MYCN amplification. The ROC curves of the NSE level, radiomic signature, and combined model are exhibited in Fig. 6, respectively.

Due to the extensive tumor heterogeneity among children with NB, the prognosis varies significantly with different stages and risk factors.[2] The MYCN gene is a significant member of the MYC oncogene family and has a strong oncogenic potential.[25] In NB with MYCN amplification, the tumor cells proliferate malignantly and spread into the blood to cause systemic metastasis in the early stage, and the higher the amplification, the worse the prognosis. In addition, MYCN amplification is closely correlated with the highly enriched blood vessels in NB, indicating that MYCN is involved in oncogenic transformation and promotes the angiogenesis and metastasis of NB. Since it is unique to the tumor and is not disturbed by external factors, the associated prognosis can be judged more accurately and independently.[26] As a tumor marker of NB, NSE is a glycolytic enzyme in the glycolysis pathway that normally exists in neurons and nerve-derived cells, and is released when the cells are destroyed. It has great clinical value in the early diagnosis of NB, and its elevation usually indicates an advanced stage and poor prognosis.[27]

Radiomics has the potential to assess the spatial heterogeneity of tumors as a non-invasive 'multiple virtual biopsy' tool.[28] The characteristics of the tumor can be comprehensively evaluated, and the accuracy of preoperative evaluation and prognosis prediction can be improved by combining radiomic features and clinical data, which has been confirmed in previous investigations.[29] In this study, we investigated the feasibility of the MRI-based radiomic signature for predicting MYCN amplification among pediatric patients with abdominal NB. The radiomic signature achieved more favorable performance than the NSE level, but the combined radiomic signature–NSE model achieved comparable performance to the signature only. Furthermore, in this study, we screened 6 features from a large set of radiomic features associated with MYCN amplification by feature selection. Among these retained features, 5 features belong to the texture feature type, including GLCM, GLRLM, and NGTDM features. These indirectly reflect NB tumor heterogeneity, suggesting a correlation between abnormal

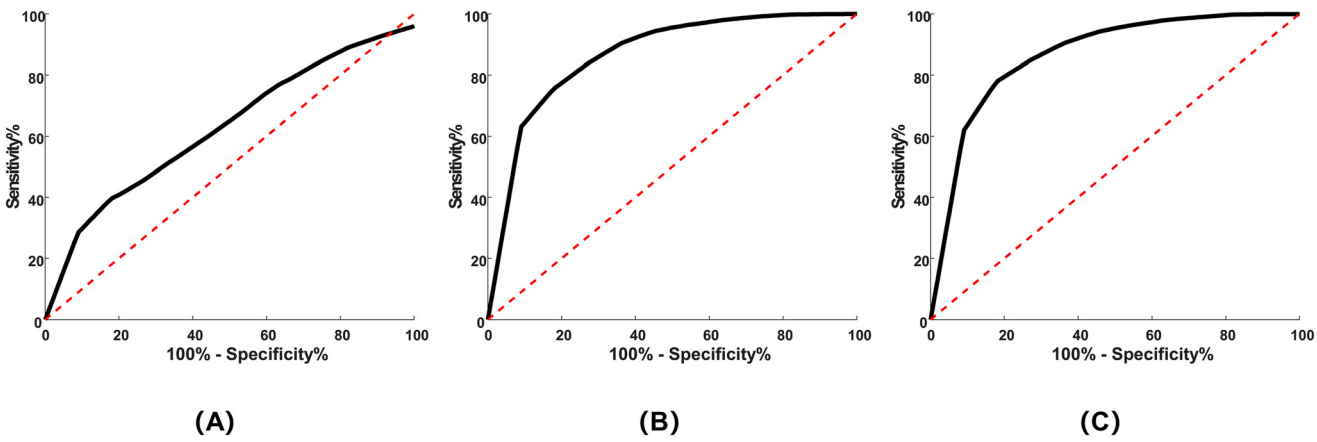

Fig. 6 ROC curves of the NSE level (A), radiomic signature (B), and combined model (C) for predicting MYCN amplification of abdominal NB.

MYCN amplification in NB patients and their poor prognoses. Although pathological biopsy is still the gold standard for diagnosing MYCN amplification at present, the radiomic signature can be used in the diagnostic workflow for cases where it is technically difficult to perform a safe biopsy or where the patient's condition is temporarily not suitable for biopsy. Predicting MYCN amplification preoperatively using routinely acquired MRI enables early identification of high-risk patients before conventional pathological biopsy results are available, which allows clinicians to expedite treatment selection and optimize surgical planning. Prompt risk-adapted therapy may improve event-free survival or overall survival in MYCN-amplified neuroblastoma patients.

There were some limitations in this study. First, although the radiomic signature based on MRI has yielded favorable performance in predicting MYCN amplification of pediatric NB, the generalizability of this finding is limited due to the small patient sample number from just one medical center. Multi-center external validation will be conducted in the future. Second, the radiomic signature was established only based on T2w MR images, other structural MRI[30] and molecular MRI can also be integrated into future studies for further improvement. Third, the choice of the classification method is critical for performance.[31] This study only used the ROC analysis method to assess the performance of the radiomic features and signature, and whether other machine learning-based models[32] have better performance was not evaluated. We will further explore machine learning-based models in the future. Last, we did not explore the correlation between the radiomic signature and endpoints with clear clinical significance, such as event-free survival, overall survival, or specific treatment response. Subsequent efforts will involve systematically collecting and integrating clinical outcome data, conducting survival analyses, and delving into the associations between the radiomic signature and prognosis.

Conclusion

In conclusion, we proposed an MRI-based radiomic signature for predicting MYCN amplification in children with abdominal NB. Our findings show that the proposed signature has achieved favorable performance, indicative of great potential as a future biomarker in NB diagnoses.

Author contributions

Xuan Jia: conceptualization, data curation, formal analysis, investigation, methodology, resources, writing – original draft. Junjie Wen: conceptualization, formal analysis, investigation, methodology, software, writing – original draft, writing – review & editing. Jiawei Liang: data curation, investigation, validation, writing – review & editing. Xiaohui Ma: data curation, methodology, validation, visualization, writing – review & editing. Wenqi Wang: data curation, formal analysis, visualization, writing – review & editing. Jinhu Wang: project administration, resources, supervision, writing – review & editing. Yi Zhang: conceptualization, project administration, resources, supervision, writing – review & editing.

Conflicts of interest

No financial or non-financial benefits have been received or will be received from any party related directly or indirectly to the subject of this article.

Data availability

Data collected from patient participants, as described in Fig. 1, are not available for ethical confidentiality requirement reasons.

Acknowledgements

The National Key Research and Development Program of China: 2023YFE0210300 and 2024YFC2707700, the Key R&D Program of Zhejiang Province: 2022C04031 and the Fundamental Research Funds for the Central Universities: 2025ZFJH01 are acknowledged. This work was supported by the "Pioneer" and "Leading Goose" R&D Program of Zhejiang Province: No. 2024C03181 and No. 2025C01106.

References

1 G. M. Brodeur, Neuroblastoma: biological insights into a clinical enigma, *Nat. Rev. Cancer*, 2003, **3**(3), 203–216.
2 J. R. Park, A. Eggert and H. Caron, Neuroblastoma: biology, prognosis, and treatment, *Pediatr. Clin. North Am.*, 2008, **55**(1), 97–120.
3 M. Huang and W. A. Weiss, Neuroblastoma and MYCN, *Cold Spring Harbor Perspect. Med.*, 2013, **3**(10), a014415.
4 K. Campbell, J. M. Gastier-Foster and M. Mann, *et al.*, Association of MYCN copy number with clinical features, tumor biology, and outcomes in neuroblastoma: A report from the Children's Oncology Group, *Cancer*, 2017, **123**(21), 4224–4235.
5 D. Mullassery, V. Sharma and A. Salim, *et al.*, Open versus needle biopsy in diagnosing neuroblastoma, *Linchuang Xiaoer Waike Zazhi*, 2014, **49**(10), 1505–1507.
6 S. L. Cohn, A. D. Pearson and W. B. London, *et al.*, The International Neuroblastoma Risk Group (INRG) classification system: an INRG task force report, *J. Clin. Oncol.*, 2009, **27**(2), 289–297.
7 P. Lambin, R. T. Leijenaar and T. M. Deist, *et al.*, Radiomics: the bridge between medical imaging and personalized medicine, *Nat. Rev. Clin. Oncol.*, 2017, **14**(12), 749–762.
8 R. J. Gillies, P. E. Kinahan and H. Hricak, Radiomics: images are more than pictures, they are data, *Radiology*, 2016, **278**(2), 563–577.
9 S. R. Digumarthy, A. M. Padole and R. L. Gullo, *et al.*, Can CT radiomic analysis in NSCLC predict histology and EGFR mutation status?, *Medicine*, 2019, **98**(1), e13963.

10 N. Taguchi, S. Oda and Y. Yokota, *et al.*, CT texture analysis for the prediction of KRAS mutation status in colorectal cancer via a machine learning approach, *Eur. J. Radiol.*, 2019, **118**, 38–43.
11 N. Pace, L. Ricci and S. Negrini, A comparison approach to explain risks related to X-ray imaging for scoliosis, 2012 SOSORT award winner, *Scoliosis*, 2013, **8**, 1–7.
12 B. H. Kushner, Neuroblastoma: a disease requiring a multitude of imaging studies, *J. Nucl. Med.*, 2004, **45**(7), 1172–1188.
13 H. W. Goo, Whole-body MRI of neuroblastoma, *Eur. J. Radiol.*, 2010, **75**(3), 306–314.
14 C. C. Swift, M. J. Eklund and J. M. Kraveka, *et al.*, Updates in diagnosis, management, and treatment of neuroblastoma, *Radiographics*, 2018, **38**(2), 566–580.
15 H. Li, Y. Zhu and E. S. Burnside, *et al.*, Quantitative MRI radiomics in the prediction of molecular classifications of breast cancer subtypes in the TCGA/TCIA data set, *npj Breast Cancer*, 2016, **2**, 16012.
16 S. J. Hectors, S. Lewis and C. Besa, *et al.*, MRI radiomics features predict immuno-oncological characteristics of hepatocellular carcinoma, *Eur. Radiol.*, 2020, **30**, 3759–3769.
17 G. Li, L. Li and Y. Li, *et al.*, An MRI radiomics approach to predict survival and tumour-infiltrating macrophages in gliomas, *Brain*, 2022, **145**(3), 1151–1161.
18 P. Ambros, I. Ambros and G. Brodeur, *et al.*, International consensus for neuroblastoma molecular diagnostics: report from the International Neuroblastoma Risk Group (INRG) Biology Committee, *Br. J. Cancer*, 2009, **100**(9), 1471–1482.
19 R. Kikinis, S. D. Pieper and K. G. Vosburgh, 3D Slicer: a platform for subject-specific image analysis, visualization, and clinical support, *Intraoperative imaging and image-guided therapy*, Springer, 2013, pp. 277–289.
20 J. J. M. Van Griethuysen, A. Fedorov and C. Parmar, *et al.*, Computational Radiomics System to Decode the Radiographic Phenotype, *Cancer Res.*, 2017, **77**(21), e104–e107, DOI: **10.1158/0008-5472.CAN-17-0339**.
21 Y. Li, S. Ammari and C. Balleyguier, *et al.*, Impact of preprocessing and harmonization methods on the removal of scanner effects in brain MRI radiomic features, *Cancers*, 2021, **13**(12), 3000.
22 M. M. Vasquez, C. Hu and D. J. Roe, *et al.*, Least absolute shrinkage and selection operator type methods for the identification of serum biomarkers of overweight and obesity: simulation and application, *BMC Med. Res. Methodol.*, 2016, **16**, 1–19.
23 S. Halligan, Y. Menu and S. Mallett, Why did European Radiology reject my radiomic biomarker paper? How to correctly evaluate imaging biomarkers in a clinical setting, *Eur. Radiol.*, 2021, **31**(12), 9361–9368.
24 X. Sun and W. Xu, Fast implementation of DeLong's algorithm for comparing the areas under correlated receiver operating characteristic curves, *IEEE Signal Process. Lett.*, 2014, **21**(11), 1389–1393.
25 E. Bell, L. Chen and T. Liu, *et al.*, MYCN oncoprotein targets and their therapeutic potential, *Cancer Lett.*, 2010, **293**(2), 144–157.
26 A. Delaidelli, G. L. Negri and A. Jan, *et al.*, MYCN amplified neuroblastoma requires the mRNA translation regulator eEF2 kinase to adapt to nutrient deprivation, *Cell Death Differ.*, 2017, **24**(9), 1564–1576.
27 D. B. Groff, Pelvic neoplasms in children, *J. Surg. Oncol.*, 2001, **77**(1), 65–71.
28 F. Giganti, S. Antunes and A. Salerno, *et al.*, Gastric cancer: texture analysis from multidetector computed tomography as a potential preoperative prognostic biomarker, *Eur. Radiol.*, 2017, **27**, 1831–1839.
29 G. A. Kaissis, S. Ziegelmayer and F. K. Lohöfer, *et al.*, Image-based molecular phenotyping of pancreatic ductal adenocarcinoma, *J. Clin. Med.*, 2020, **9**(3), 724.
30 M. Iv, M. Zhou and K. Shpanskaya, *et al.*, MR imaging–based radiomic signatures of distinct molecular subgroups of medulloblastoma, *Am. J. Neuroradiol.*, 2019, **40**(1), 154–161.
31 X. Gao, T. Ma and S. Bai, *et al.*, A CT-based radiomics signature for evaluating tumor infiltrating Treg cells and outcome prediction of gastric cancer, *Ann. Transl. Med.*, 2020, **8**(7), 469.
32 H. C. Kniep, F. Madesta and T. Schneider, *et al.*, Radiomics of brain MRI: utility in prediction of metastatic tumor type, *Radiology*, 2019, **290**(2), 479–487.